Metallography, Microstructure, and Analysis (2024) 13:307–316
https://doi.org/10.1007/s13632-024-01056-3

ORIGINAL RESEARCH ARTICLE

Achieving Unusual Stable Textures in AZ91 Alloy by Asymmetric Hot Rolling

Ebrahim Tolouie[1] · Roohollah Jamaati[1]

Received: 2 December 2023 / Revised: 5 February 2024 / Accepted: 11 February 2024 / Published online: 28 February 2024

Abstract

⟨0001⟩||RD-oriented AZ91 magnesium alloy was produced by asymmetric hot rolling (AHR). The corresponding microstructures and texture evolutions were investigated. It was found twinning acts as an important role at the beginning of the plastic deformation. There were no obvious recrystallization mechanisms in 8% deformed AZ91; on the contrary, partial recrystallization (PSN mode) occurred during 15% hot rolling. Since ⟨0001⟩ of many grains were parallel to the RD, the Schmid factor of basal slip was about 0, and it was hard to activate basal slip during 8% rolling. It was of special interest to observe that the intensity of basal orientation significantly enhanced from 2.6×R to 47.7×R (the letter R means multiple of random distribution) with an increase in the rolling deformation from 8% to 15%. Both extension twinning and {0001} basal slip reoriented the {0001} planes perpendicular to the axis of compression during 15% rolling. In the 15% deformed sample, the increased activity of pyramidal slip led to a splitting of the {0001} pole in the rolling direction. Interestingly, the AZ91 sheets produced by AHR exhibited some unusual stable textures such as $\{30\overline{3}1\}$ ||ND,$\{11\overline{2}4\}$ ||ND, $\{01\overline{1}0\}\langle\overline{2}110\rangle$, and $\{01\overline{1}0\}\langle\overline{2}11\overline{6}\rangle$. The fiber textures indicated that the {0001}||ND and $\{11\overline{2}4\}$ ||ND fibers were the end and intermediate orientations in the hot-rolled AZ91 alloy.

Keywords Texture · Magnesium alloy · Asymmetric hot rolling

Introduction

Magnesium alloys are potential candidates for automotive, aerospace, and electronic industries owing to their low density, high strength-to-density and stiffness, electromagnetic shielding, high heat dissipation, and recycling advantages [1–3]. However, because of the limited slip systems of HCP crystalline structure, the rolled magnesium usually reveals a strong {0002} texture where the grains' c-axis is aligned parallel to the normal direction (ND). This preferred orientation will result in low ductility at ambient temperature and strong anisotropy, which consequently limits their application [4–8]. Thus, many attempts were made to modify the texture of Mg alloys via different methods. Large strain rolling [9–11], cross rolling [12–15], and asymmetric rolling [16–18] have been indicated to enhance the ductility of Mg slightly at ambient temperature by a little inclination of basal texture. This inclination was ascribed to the pyramidal slip and double twinning [19].

Xu et al. [20] stated that a large rolling deformation in the final stages of hot rolling increases the fraction of recrystallized grains in the microstructure and decreases the intensity of the {0001} orientation of magnesium-rare earth alloys, which leads to the enhancement of the ductility. Huang et al. [21] investigated the impact of rolling deformation per pass on the textural and microstructural evolution of an Mg-3Al-1Zn alloy by asymmetric rolling. It was found that the direction of inclination of the {0001} pole with respect to the rolling direction depended on the rolling strain per pass. Ferdowsi et al. [22] reported that for the Mg-9Al-1Zn alloy, the plastic strain applied during low-temperature rolling was accommodated by the generation of shear bands and twins, while during high-temperature rolling, non-basal slip systems were activated leading to the twinning inhibition; therefore, slip became the dominant mechanism of plastic deformation.

Too little attention is paid to modifying the texture of Mg alloys by asymmetric rolling, especially for AZ91 alloy. On

✉ Roohollah Jamaati
jamaati@nit.ac.ir

1 Department of Materials Engineering, Babol Noshirvani University of Technology, Shariati Ave., Babol 47148–71167, Iran

the other hand, it was found that a combination of extension twinning and basal slip is responsible for the high-intensity {0001} texture in the rolled magnesium alloys [1–8]. Therefore, the presence of an initial texture such as ⟨0001⟩||RD, which is inappropriate for basal slip, may alter the texture commonly produced by rolling. However, the impact of initial ⟨0001⟩||RD orientation on the textural and microstructural evolutions of AZ91 alloys during the rolling was not studied. The objective of this work is to systematically investigate the influence of initial strong ⟨0001⟩||RD on the texture and microstructure of the asymmetrically hot-rolled Mg-9Al-1Zn alloy sheets with different rolling reductions.

Materials and Methods

The as-received material was an as-cast Mg–8.43Al–1.27Zn–0.29Mn alloy with 3.5 mm thickness. The alloy was heat-treated at 723 K for 24 h before asymmetric rolling. Then, the samples were pre-heated (at 673 K for 600 s) and asymmetrically rolled with strains of 8% and 15%. Cold deformation was conducted on a laboratory rolling mill with 150 mm in diameter. The asymmetric rolling technique used in the current research was the single-roll drive (SRD) mode, and the speed of the down roller was fixed at 50 rpm.

The microstructural evolution of samples was examined by an optical microscope on the RD–TD section. The etchant was a 4.6 g picric acid + 10 ml acetic acid + 10 ml distilled H_2O + 70 ml ethanol. The macrotextures were measured by X-ray diffraction (XRD) at the ¼ thickness of the sheets on the RD-TD section. Incomplete {0002} and $\{10\bar{1}0\}$ pole figures (PFs) were used to calculate the orientation distribution function (ODF) by the TexTools software. The calculation of ODF from incomplete pole figures can be performed by an iterative procedure taking into account the positivity condition for all PFs. This technique strongly decreases instabilities which may occasionally take place in other techniques. Using the ODF, it is possible to obtain fiber textures and texture components in the rolled samples.

Results and Discussion

Optical micrographs of the initial and hot-rolled sheets are shown in Fig. 1. The boundaries can be classified by different neighbor misorientations: low-angle boundary (LAB, 0°–15°), high-angle boundary (HAB, 15°–65°), and extra high-angle boundary (EHAB, 65°–100°). The relationship between the fraction of three different boundaries and the rolling reduction is shown in Fig. 2. Figure 1a displays a micrograph of the homogenized sheet featuring homogeneously distributed equiaxed alpha grains. A mean grain size

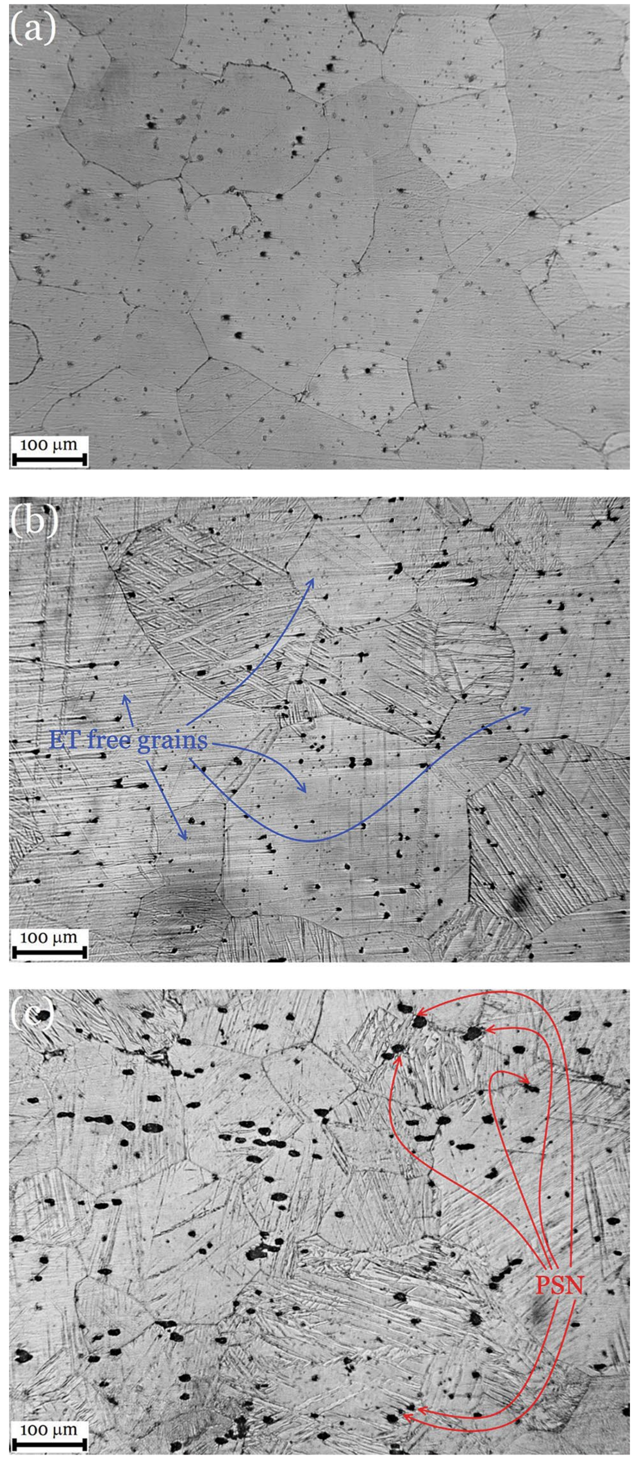

Fig. 1 The microstructures of **a** 0% (homogenized), **b** 8%, and **c** 15% hot-rolled AZ91. The extension twins are thick. Some small grains (as displayed by red arrows in Fig. 1(**c**)) are nucleated adjacent to the particles through the PSN

of 125 µm calculated by the linear intercept method, where the grain size varies within the range from 60 µm to 150 µm. Due to the homogenization treatment of the as-cast sheet, the

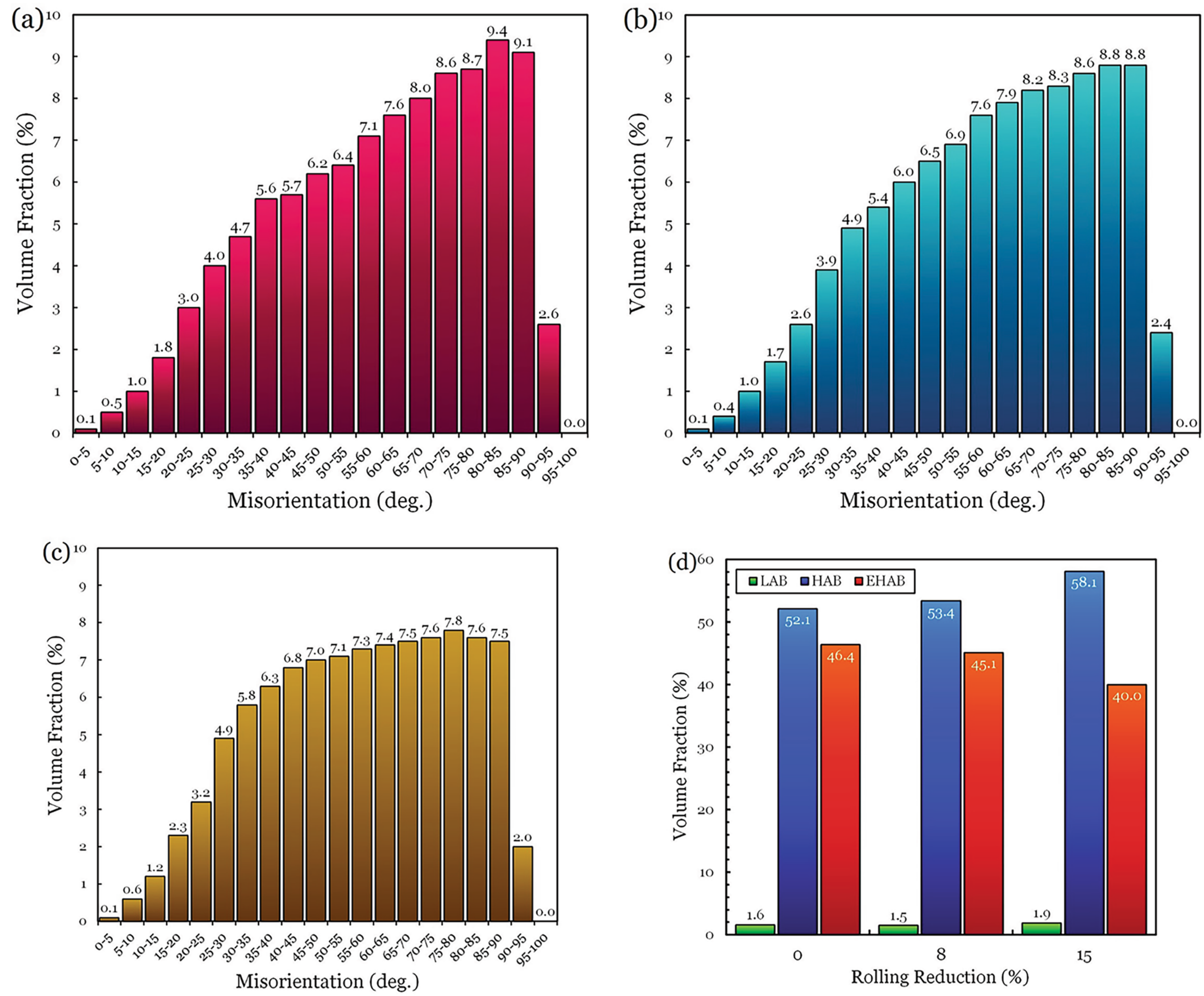

Fig. 2 The misorientation distributions of **a** 0% (homogenized), **b** 8%, and **c** 15% hot-rolled AZ91, and **d** the volume fraction of LAB, HAB, and EHAB for different samples

amount of $Mg_{17}Al_{12}$ intermetallic compounds decreases and a large fraction of EHABs (46.4%) is generated. There is no evidence of twinning in the microstructure of the homogenized sheet. After the 8% hot deformation (Fig. 1b), the microstructure of AZ91 changes from the fully homogenized structure to the deformed structure, containing several twins. The fraction of HABs increases to 53.4% while that of EHABs decreases to 45.1% by 8% hot rolling (see Fig. 2). A large number of thick $\{10\overline{1}2\}$ twins are observed in Fig. 1b. Also, a few thin $\{10\overline{1}1\}$ contraction twins and/or $\{10\overline{1}1\} - \{10\overline{1}2\}$ double twins are also presented in the sample after 8% rolling. As revealed in Fig. 1b, twinning plays a main role in the beginning of the plastic deformation. The critical resolved shear stress (CRSS) for extension twinning for Mg alloys is lower than that of contraction twinning [6, 17, 18]. However, there are no extension twins inside some grains as displayed by blue arrows in Fig. 1b. This is due to the unfavorable orientation of these grains for extension twinning. This twinning easily occurs under compression perpendicular to the grains' c-axis or under tensile parallel to the grains' c-axis. For the 8% deformed sample, the grain size is ~ 122 µm, which is similar to that before the hot rolling process. This suggests no occurrence of dynamic recrystallization (DRX) during the deformation of the AZ91 alloy. Since strain stored energy in the rolled AZ91 is low under 8% deformation, it is difficult for new grains to nucleate. The 15% deformed sample contains a very large amount of twins in the microstructure as demonstrated in Fig. 1c. No sign of DRX is seen in the micrograph of this sample. However, some small grains (as displayed by red arrows) are nucleated adjacent to the particles through the particle-stimulated nucleation (PSN) mechanism during preheat treatment and/or rolling. As depicted in Fig. 2, the fraction of the LABs and HABs increases to 1.9% and 58.1%, respectively, and the EHABs fraction decreases to 40.0% when the deformation increases to 15%. Based on the obtained results, DRX is almost inhibited during deformation because the initial samples were just preheated and rolled by cold mills. Since the dimensions of the samples were much lower than the rolling mills, the rate of the temperature decrease became markedly fast. In fact, recrystallization has almost no effect on the preferred orientation of rolled AZ91 samples. Therefore, it can be concluded that the texture evolution is related to the slip and twinning mechanisms. Also, with an increase in the rolling reduction, the size of $Mg_{17}Al_{12}$ particles increases. This is due to both the pre-heat treatment and the hot deformation.

Figure 3 shows recalculated {0002} pole figures of the heat-treated and hot-deformed samples. The ODF of the samples after different thickness reductions is illustrated in Fig. 4. Figure 3a shows there is no basal texture in the homogenized sample. From Fig. 4a, two strong textures ($\{10\bar{1}0\}\langle 0001\rangle$ and $\{11\bar{2}3\}\langle 10\bar{1}0\rangle$) exist in homogenized AZ91 with the intensity of 36.1 × R (multiples of random distribution, MRD). The main plastic deformation mechanisms in Mg alloys are basal slip, $\{10\bar{1}0\}\langle 11\bar{2}0\rangle$ prismatic slip, $\{10\bar{1}1\}\langle 11\bar{2}0\rangle$ and $\{11\bar{2}2\}\langle 11\bar{2}3\rangle$ pyramidal slips, and $\{10\bar{1}2\}\langle 10\bar{1}1\rangle$ extension twinning, $\{10\bar{1}1\}\langle 10\bar{1}2\rangle$ contraction twinning as well as $\{10\bar{1}1\} - \{10\bar{1}2\}$ double twinning [6, 17, 18]. The rotation of grains due to slip and the formation of twins during plastic deformation lead to the formation of a preferred orientation. In this work, variations in plastic deformation mechanisms can be interpreted in terms of the effect of the original orientation on twinning and slip. Since ⟨0001⟩ of many grains is parallel to the RD, the Schmid factor of {0001} slip is ~ zero, and it is hard for the activation of {0001} slip in the rolling. For these grains, extension twinning is the initial mode of deformation. Also, for $\{11\bar{2}3\}\langle 10\bar{1}0\rangle$ oriented grains and others, the {0001} slip is the main deformation mechanism during the early deformation stage. After 8% thickness reduction (Fig. 3b), the pole figure has only a weak {0002} fiber texture. As seen in Fig. 3b, after 8% deformation the texture is made up of two new fiber textures $\{10\bar{1}0\}$ ||ND and $\{11\bar{2}0\}$ ||ND. Figure 4b shows that there are some strong components such as $\{01\bar{1}0\}\langle\bar{2}110\rangle$, $\{11\bar{2}0\}\langle\bar{2}20\bar{1}\rangle$, and $\{01\bar{1}1\}\langle\bar{5}32\bar{1}\rangle$ with the intensity of 40.6 × R, 30.9 × R, and 29.6 × R, respectively.

The original grains with non-basal orientation quickly rotate to the basal texture by a low amount of deformation [23–28]. However, in this work, there was a weak basal texture after 8% rolling. This is ascribed to the original strong ⟨0001⟩||RD orientation, which is not favored for both prismatic and basal slips. Since the Schmid factor for the {0001}

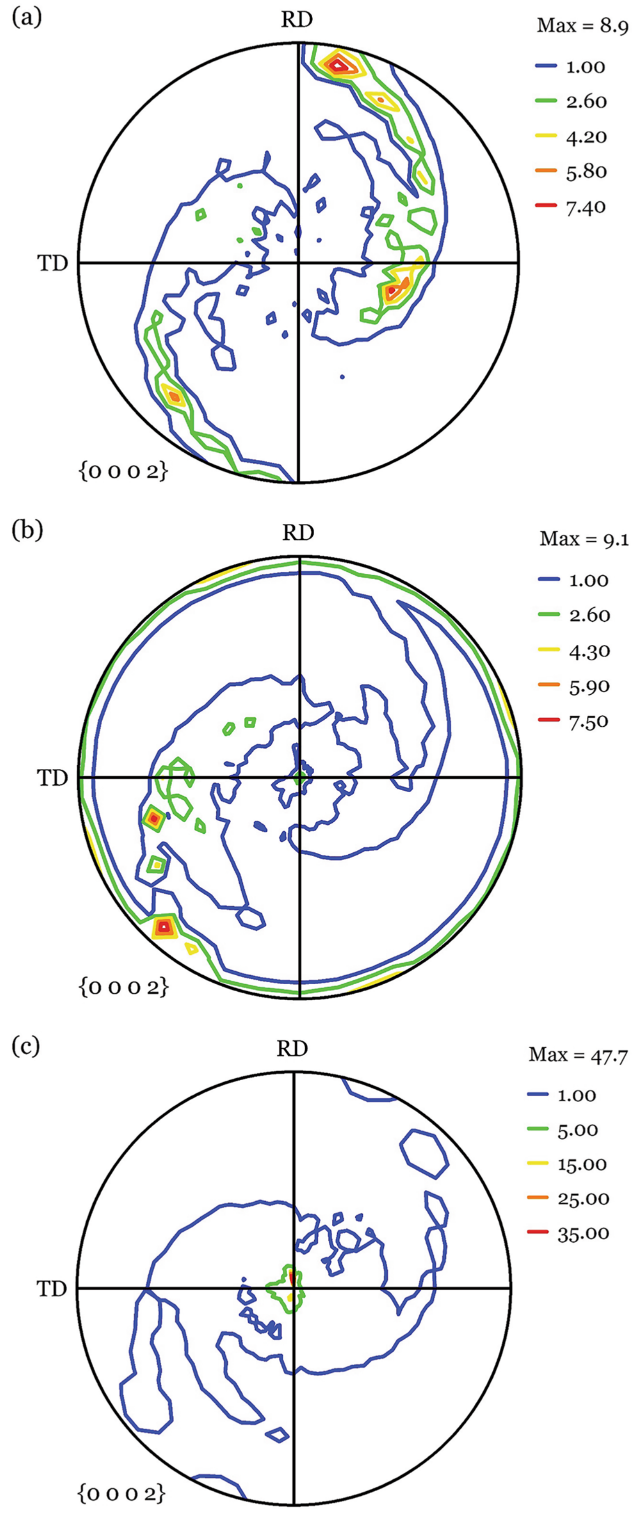

Fig. 3 The {0002} pole figures of **a** 0% (homogenized), **b** 8%, and **c** 15% hot-rolled AZ91

slip of grains with the c-axis perpendicular and parallel to the direction of applied loading is ~ zero, basal and prismatic slips will be hindered. Since basal slip is the most important

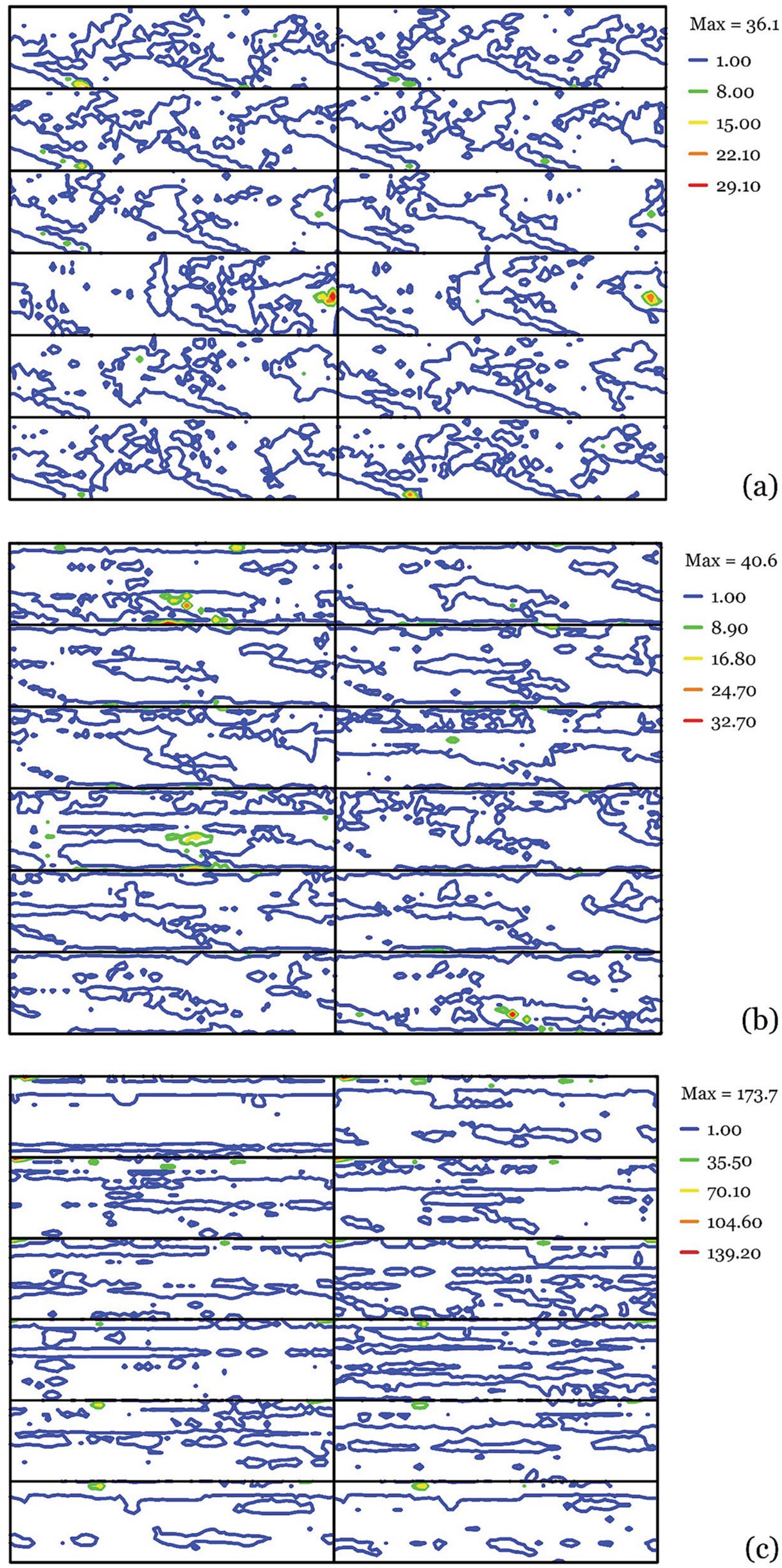

Fig. 4 The ODFs of **a** 0% (homogenized), **b** 8%, and **c** 15% hot-rolled AZ91

factor in the generation of strong basal orientation, the weak basal texture after 8% deformation is related to suppressing the basal slip. However, the basal orientation strengthened during 8% rolling. This is due to the occurrence of pyramidal slip and extension twinning.

As depicted in Fig. 1b, a large number of $\{10\bar{1}2\}$ extension twins is observed at a low degree of deformation.

These twins mainly formed in the grains with their c-axis perpendicular to the ND. Owing to the rotation of the {0001} by 86.3° during the extension twinning, the twinned area tended to have its c-axis parallel to the ND, and {0001} texture was created as a result of the extension twinning.

Besides the effect of extension twinning due to the initial ⟨0001⟩||RD texture, the activation of pyramidal ⟨c + a⟩ slip may be one reason responsible for increasing the intensity of basal orientation for the 8% deformed AZ91 alloy. On the one hand, the pyramidal slip may be activated to some extent owing to the hot deformation. On the other hand, the strong ⟨0001⟩||RD orientation may increase the activity of pyramidal slip during plastic deformation owing to its high Schmid factor. Therefore, the activation of pyramidal slip is necessary to fulfill the strain demand. This kind of slip can be activated under the compressive load along the c-axis or the tensile load perpendicular to the c-axis. Therefore, pyramidal slip decreases the contribution of {0001} slip. For this reason, the {0002} orientation during 8% deformation slightly increased.

As shown in Fig. 3b, 15% hot deformation leads to a significant strengthening of basal orientation with an enhancement in the intensity from 2.6 × R to 47.7 × R and a replacement of a single peak by a double one in the basal pole. This is not observed in AZ91 samples processed by low-strain hot rolling. At least two reasons may explain the very strong basal texture after 15% deformation:

(1) At the beginning of the rolling, extension twinning is easily activated owing to the presence of ⟨0001⟩||RD orientation. By further increase in strain, the matrix is consumed and reoriented by extension twinning, which contributes to the generation of basal orientation.

(2) Twinning became an important mechanism of deformation in the 8% rolled AZ91 alloy; however, higher strains need additional deformation by slip. It should be noted that asymmetric rolling can activate the basal slip at higher deformation. As a result of the higher effective strain (i.e., 15%) and continuously rotating principle normal axis through the asymmetric hot rolling, which promotes the activation of basal slip system in the ⟨0001⟩||RD oriented grains during deformation. Consequently, both {0001} slip and extension twinning reorient the {0001} perpendicular to the axis of compression during 15% strain.

In the 15% deformed sample, the distribution of basal poles demonstrated a basal texture with a splitting along the RD. The double-intensity peaks tilted about 4.6° from the ND to the RD. At high temperatures, the CRSS of pyramidal slips decreases, especially pyramidal ⟨c + a⟩ slip, which tends to split the basal intensity toward RD.

As seen in Fig. 4c, there are some unexpected stable textures such as $\{30\bar{3}1\}$ ||ND and $\{11\bar{2}4\}$ ||ND fibers and also $\{01\bar{1}0\}\langle\bar{2}110\rangle$ and $\{01\bar{1}0\}\langle\bar{2}11\bar{6}\rangle$ components with the intensity of 5.8 × R and 11.2 × R, respectively. This interesting result is in contrast to the texture change reported by most researchers [22, 29–32] in their rolled AZ91 alloys, where a single strong {0002} basal texture was produced. To find the reason why the unusual fibers and components existed in the 15% deformed AZ91, a further investigation was performed using fiber textures.

The important fiber textures including {0001}||ND, $\{10\bar{1}0\}$ ||ND, $\{11\bar{2}4\}$ ||ND, $\{30\bar{3}1\}$ ||ND, and $\langle11\bar{2}0\rangle$ ||RD are presented in Figs. 5, 6, 7, 8, and 9, respectively. As seen in Fig. 5, the {0001}||ND fiber includes important components of $\{0001\}\langle10\bar{1}0\rangle$, $\{0001\}\langle11\bar{2}0\rangle$, and $\{0001\}\langle4\bar{5}10\rangle$.

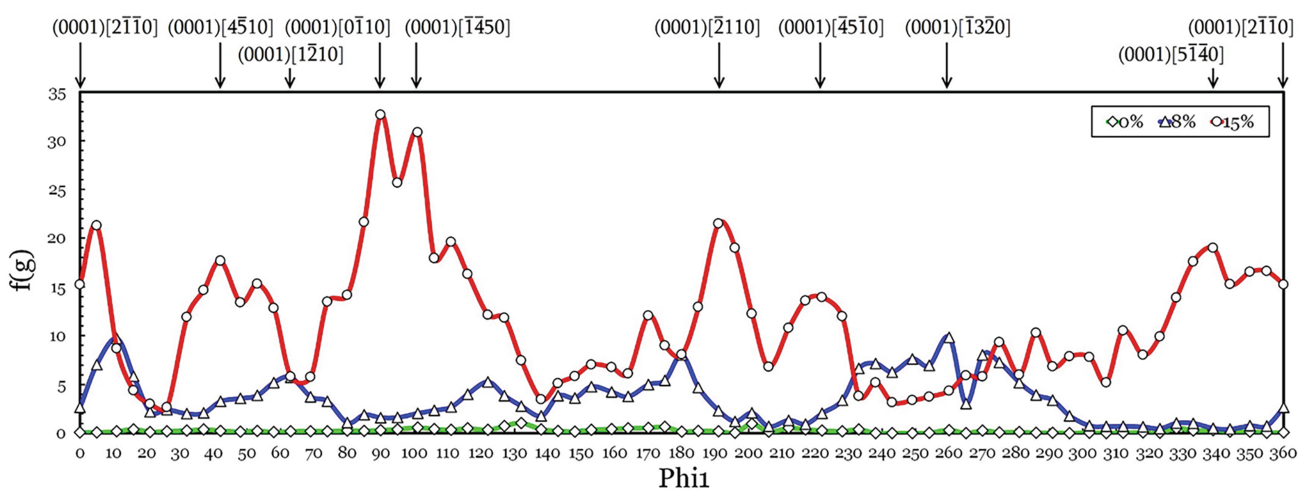

Fig. 5 The variations of {0001}||ND fiber during the hot rolling process of the AZ91 alloy

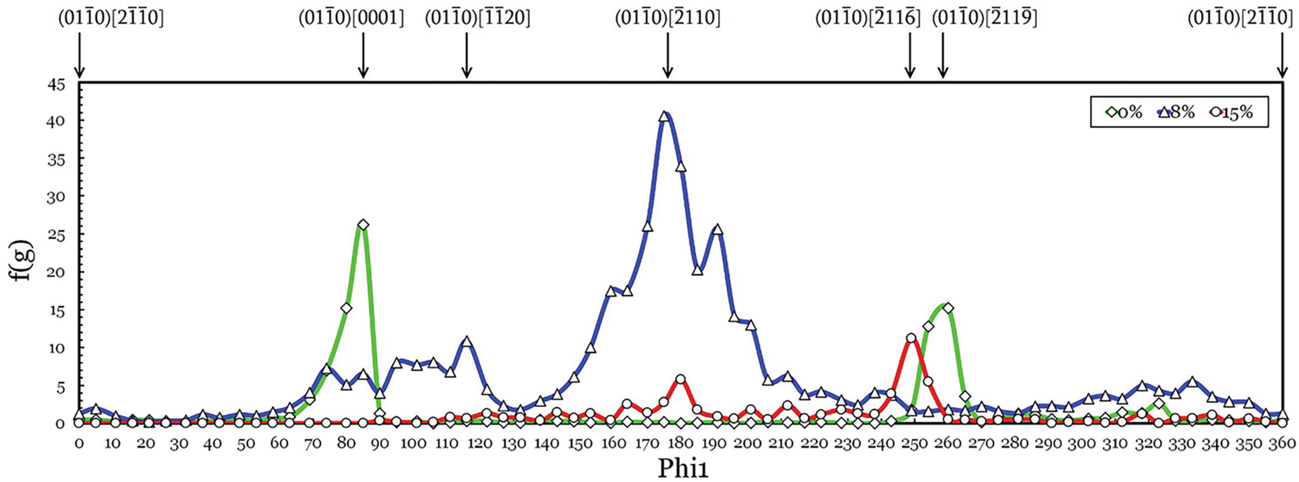

Fig. 6 The variations of {10$\bar{1}$0} ||ND fiber during the hot rolling process of the AZ91 alloy

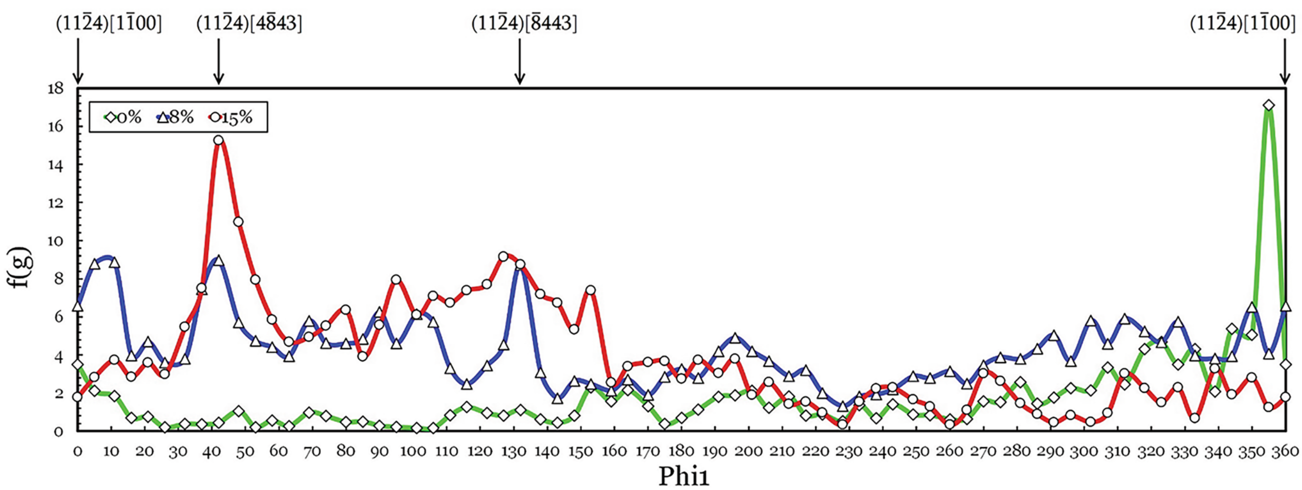

Fig. 7 The variations of {11$\bar{2}$4} ||ND fiber during the hot rolling process of the AZ91 alloy

The overall intensity of {0001}||ND fiber in the initial samples is very weak. After 8% deformation, the {0001}||ND fiber $\Phi = 0°$ strengthens. The orientation density of the {0001}||ND fiber in this sheet is mainly centered on the {0001}⟨11$\bar{2}$0⟩ and {0001}⟨12$\bar{3}$0⟩ components. With the strain up to 15%, the overall intensity of {0001}||ND fiber significantly increases. In this sample, the {0001}||ND fiber transforms from $\Phi = 0°$ to $\Phi = 14°$. The initial {0001}⟨12$\bar{3}$0⟩ orientation at $\varphi_1 = 260°$ tends to move toward the {0001}⟨4$\bar{5}$10⟩ at $\varphi_1 = 220°$ and $\varphi_1 = 340°$ by a 40° or an inversely 80° rotation around the ND (φ_1, Φ, and φ_2 are the Euler angles). On the other hand, a very strong component, i.e., {0001}⟨10$\bar{1}$0⟩ with the intensity of 32.7 × R, appears. In addition, the pre-existed {0001}⟨11$\bar{2}$0⟩ orientation strengthens from 9.7 × R to 23.6 × R. These results suggested that the {0001}||ND fiber is an end orientation in the hot-rolled AZ91 alloy.

From Fig. 6, the {10$\bar{1}$0} ||ND comprises {10$\bar{1}$0}⟨11$\bar{2}$0⟩, {10$\bar{1}$0}⟨0001⟩, {10$\bar{1}$0}⟨$\bar{2}$11$\bar{9}$⟩, and {10$\bar{1}$0}⟨$\bar{2}$11$\bar{6}$⟩ components. The distribution of orientation density along the {10$\bar{1}$0} ||ND fiber for all sheets is not uniform. The orientation density of this fiber in the as-homogenized AZ91 sample is mainly centered on the {10$\bar{1}$0}⟨0001⟩ and {10$\bar{1}$0}⟨$\bar{2}$11$\bar{9}$⟩ component with the intensity of 26.2 × R and 15.2 × R, respectively. After 8% hot rolling, the intensity of {10$\bar{1}$0} ||ND fiber increases. Also, the pre-existed {10$\bar{1}$0}⟨0001⟩ and {10$\bar{1}$0}⟨$\bar{2}$11$\bar{9}$⟩ orientations at $\varphi_1 = 85°$ and $\varphi_1 = 260°$ directly converge toward {10$\bar{1}$0}⟨11$\bar{2}$0⟩ component at $\varphi_1 = 180°$, respectively, by a 95° or an inversely 80° rotation around the ND. After 15% deformation, the {10$\bar{1}$0} ||ND fiber weakens. It can be concluded that the {10$\bar{1}$0} ||ND fiber is an

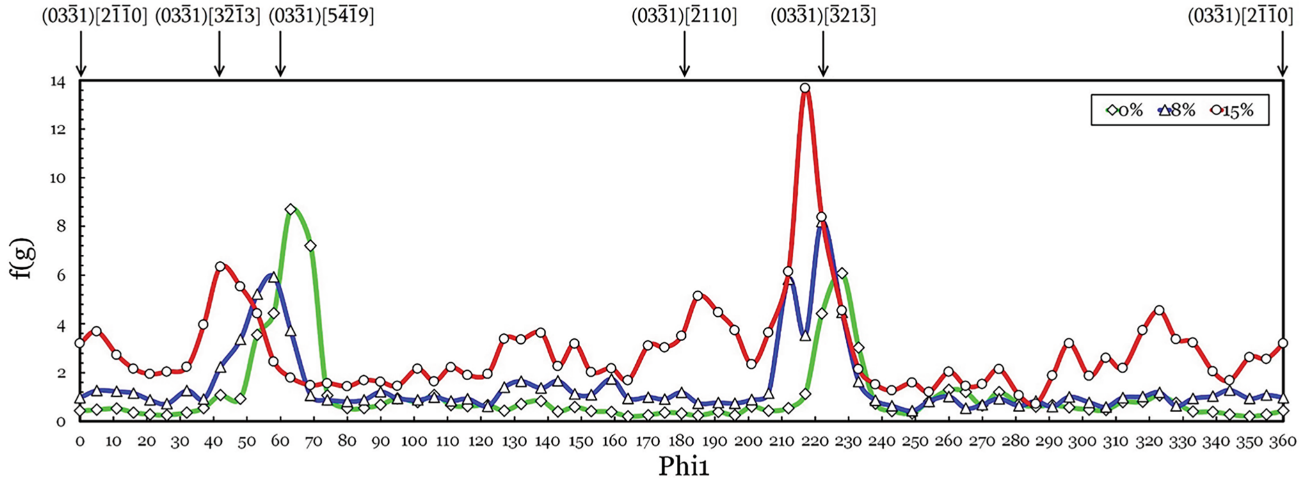

Fig. 8 The variations of $\{30\bar{3}1\}$ ||ND fiber during the hot rolling process of the AZ91 alloy

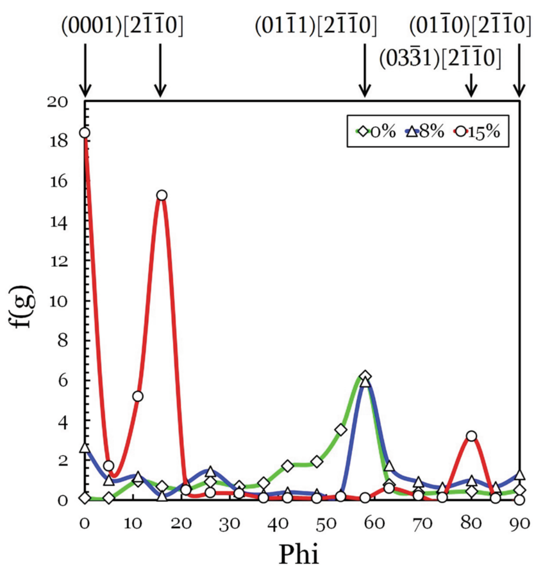

Fig. 9 The variations of $\langle 11\bar{2}0\rangle$ ||RD fiber during the hot rolling process of the AZ91 alloy

intermediate orientation in the hot-rolled AZ91 alloy. There are two main components, $\{10\bar{1}0\}\langle\bar{2}11\bar{6}\rangle$ and $\{10\bar{1}0\}\langle 11\bar{2}0\rangle$, with intensity of $11.2\times R$ and $5.8\times R$, respectively.

From Fig. 8, the $\{11\bar{2}4\}$ ||ND fiber comprises $\{11\bar{2}4\}\langle 10\bar{1}0\rangle$ and $\{11\bar{2}4\}\langle 44\bar{8}3\rangle$ components. The distribution of orientation density along the $\{11\bar{2}4\}$ ||ND fiber for all sheets is almost homogeneous. The orientation density of the $\{11\bar{2}4\}$ ||ND fiber in the initial sheet is mainly centered on the $\{11\bar{2}4\}\langle 10\bar{1}0\rangle$ orientation with an intensity of $17.1\times R$. The initial strong $\{11\bar{2}4\}\langle 10\bar{1}0\rangle$ orientation quickly weakens by increasing the deformation to 8%. However, the overall intensity of $\{11\bar{2}4\}$ ||ND fiber increases. After 15% deformation, the main component along the $\{11\bar{2}4\}$ ||ND fiber is $\{11\bar{2}4\}\langle 44\bar{8}3\rangle$ with the maximum intensity of $15.2\times R$. The first part of the $\{11\bar{2}4\}$ ||ND fiber (between $\varphi_1=0°$ and $\varphi_1=180°$) strengthens and the second part (between $\varphi_1=180°$ and $\varphi_1=360°$) weakens by 15 % hot rolling. It can be said that, unlike the $\{0001\}$||ND and $\{10\bar{1}0\}$ ||ND fibers, the orientation distribution along the $\{11\bar{2}4\}$ ||ND fiber is not remarkably altered by asymmetric hot rolling.

Orientations of the $\{30\bar{3}1\}$ ||ND fiber are distributed at (φ_1, 80°, 0°) in the Euler space (Fig. 8). The orientation density of this fiber is mainly centered on $\{30\bar{3}1\}\langle 12\bar{3}3\rangle$, $\{30\bar{3}1\}\langle 14\bar{5}9\rangle$, and $\{30\bar{3}1\}\langle 11\bar{2}0\rangle$ components. As seen, the $\{30\bar{3}1\}\langle 14\bar{5}9\rangle$ and $\{30\bar{3}1\}\langle 12\bar{3}3\rangle$ are the strongest orientations along the $\{30\bar{3}1\}$ ||ND fiber with the intensity of $8.7\times R$ and $6.1\times R$, respectively. After an 8% rolling reduction, the main textures are similar to the initial sample. However, the $\{30\bar{3}1\}\langle 12\bar{3}3\rangle$ component is stronger in intensity than the $\{30\bar{3}1\}\langle 14\bar{5}9\rangle$ orientation ($8.4\times R$ vs. $5.9\times R$). Therefore, a texture transition from $\{30\bar{3}1\}\langle 14\bar{5}9\rangle$ to $\{30\bar{3}1\}\langle 12\bar{3}3\rangle$ occurs during the 8% deformation of the AZ91 alloy. Finally, with the strain up to 15%, the $\{30\bar{3}1\}\langle 14\bar{5}9\rangle$ orientation converges toward $\{30\bar{3}1\}\langle 12\bar{3}3\rangle$ component at $\varphi_1=40°$. In addition, the $\{30\bar{3}1\}\langle 12\bar{3}3\rangle$ orientation at $\varphi_1=220°$ becomes stronger ($13.7\times R$). Moreover, a new component, i.e., $\{30\bar{3}1\}\langle 11\bar{2}0\rangle$, with the intensity of $5.2\times R$ created by 15% deformation. From Fig. 8, with an increase in the reduction in thickness, the overall intensity of $\{30\bar{3}1\}$ ||ND fiber increases.

From Fig. 9, the overall intensity of $\langle 11\bar{2}0\rangle$ ||RD texture for all sheets is almost weak and the distribution of orientation density along this fiber is not homogeneous. The main textures along the $\langle 11\bar{2}0\rangle$ ||RD fiber are $\{0001\}\langle 11\bar{2}0\rangle$,

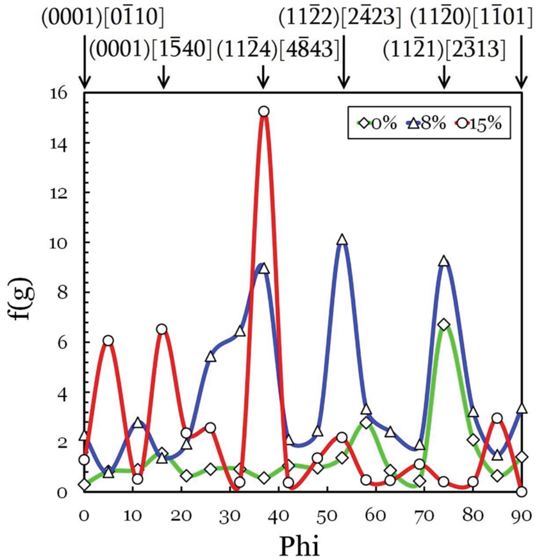

Fig. 10 The variations of new fiber (50°,Φ,45°) during the hot rolling process of the AZ91 alloy

$\{10\bar{1}1\}\langle 11\bar{2}0\rangle$, and $\{30\bar{3}1\}\langle 11\bar{2}0\rangle$ components. The orientation density of the $\langle 11\bar{2}0\rangle$ ||RD texture in the initial sheet is mainly centered on the $\{10\bar{1}1\}\langle 11\bar{2}0\rangle$ orientation with the intensity of 6.2 × R. After 8% rolling reduction, a new weak orientation, i.e., $\{0001\}\langle 11\bar{2}0\rangle$ (2.7 × R), is generated. During 15% hot deformation, the $\{10\bar{1}1\}\langle 11\bar{2}0\rangle$ orientation tends to move toward the $\{0001\}\langle 11\bar{2}0\rangle$ and also $\{30\bar{3}1\}\langle 11\bar{2}0\rangle$ at $\Phi = 80°$ by a 20° rotation around the RD. This behavior occurs at different φ_1 (from 0° to 360°); therefore, $\{30\bar{3}1\}$ ||ND fiber as an unusual texture is formed.

With regard to Fig. 4, it can be introduced a new fiber distributed at (50°,Φ,45°) in the Euler space (see Fig. 10). The distribution of orientation density along this fiber for all sheets is completely heterogeneous. As seen, the orientation density of this new fiber is mainly centered on $\{0001\}\langle 10\bar{1}0\rangle$, $\{0001\}\langle 4\bar{5}10\rangle$, $\{11\bar{2}4\}\langle 44\bar{8}3\rangle$, $\{11\bar{2}2\}\langle 22\bar{4}3\rangle$, $\{11\bar{2}1\}\langle 12\bar{3}3\rangle$, and $\{11\bar{2}0\}\langle 10\bar{1}1\rangle$ components. As seen, for the initial sample the $\{11\bar{2}1\}\langle 12\bar{3}3\rangle$ orientation is the strongest orientation of the new fiber with an intensity of 6.7 × R. By 8% hot rolling, this component strengthens to 9.3 × R. Also, two new components ($\{11\bar{2}2\}\langle 22\bar{4}3\rangle$ and $\{11\bar{2}4\}\langle 44\bar{8}3\rangle$ with the intensity of 10.1 × R and 9 × R, respectively) are created. With a thickness reduction of up to 15%, the $\{11\bar{2}1\}\langle 12\bar{3}3\rangle$ and $\{11\bar{2}2\}\langle 22\bar{4}3\rangle$ orientations converge toward $\{11\bar{2}4\}\langle 44\bar{8}3\rangle$ component. In addition, the pre-existed $\{11\bar{2}4\}\langle 44\bar{8}3\rangle$ orientation moves to $\{0001\}\langle 4\bar{5}10\rangle$ and $\{0001\}\langle 10\bar{1}0\rangle$ components at $\Phi = 15°$ and $\Phi = 5°$, respectively. It can be concluded the unexpected $\{11\bar{2}4\}$ ||ND fiber is an intermediate texture and by increasing the deformation onward 15%, it may be eliminated.

Conclusions

Textural and microstructural evolutions in hot-rolled AZ91 alloy were investigated. The main conclusions are as follows:

1. At the beginning of hot deformation, twinning took place in the AZ91 alloy.
2. There was no obvious sign of DRX. However, some small grains were observed that nucleate adjacent to the particles via the PSN during preheat treatment and/or rolling.
3. The preferred orientation of the starting material was $\langle 0001\rangle$||RD, while that of the hot-rolled sample was characterized by $\langle 0001\rangle$||ND texture.
4. Since $\langle 0001\rangle$ of many grains were parallel to the RD, the Schmid factor of {0001} slip was ~ zero, and it was hard for the activation of basal slip during 8% deformation.
5. The intensity of {0002} orientation remarkably enhanced with growing thickness reductions. Both extension twinning and {0001} slip reoriented the {0001} perpendicular to the axis of compression during 15% rolling.
6. Basal texture splitting along the rolling direction formed in a 15% deformed sample due to pyramidal $\langle c + a\rangle$ slip.
7. There is some unexpected stable texture such as $\{30\bar{3}1\}$ ||ND and $\{11\bar{2}4\}$ ||ND fibers and also $\{01\bar{1}0\}\langle\bar{2}110\rangle$ and $\{01\bar{1}0\}\langle\bar{2}11\bar{6}\rangle$ components after 15% deformation.
8. The fiber textures indicated that the {0001}||ND and $\{11\bar{2}4\}$ ||ND fibers were the end and intermediate orientations in the hot-rolled AZ91 sheet.

Data Availability All data included in this study are available upon request by contact with the corresponding author.

References

1. E Tolouie R Jamaati 2016 Effect of β-Mg17Al12 phase on microstructure, crystallographic texture, and mechanical behavior of Mg-9Al-1Zn alloy processed by asymmetric cold rolling Mater. Des. 93 194 202
2. F Yousefpour R Jamaati H Jamshidi Aval 2021 Effect of traverse and rotational speeds on microstructure, texture, and mechanical properties of friction stir processed AZ91 alloy Mater. Charact. 178 111235
3. X Li W Qi 2013 Effect of initial texture on texture and microstructure evolution of ME20 Mg alloy subjected to hot rolling Mater. Sci. Eng. A 560 321 331
4. E Tolouie R Jamaati 2019 Asymmetric cold rolling: a technique for achieving non-basal textures in AZ91 alloy Mater. Lett. 249 143 146
5. F Yousefpour R Jamaati H Jamshidi Aval 2022 Investigation of microstructure, crystallographic texture, and mechanical behavior

of magnesium-based nanocomposite fabricated via multi-pass FSP for biomedical applications J. Mech. Behav. Biomed. Mater. 125 104894
6. N Stanford K Sotoudeh PS Bate 2011 Deformation mechanisms and plastic anisotropy in magnesium alloy AZ31 Acta Mater. 59 4866 4874
7. F Yousefpour R Jamaati H Jamshidi Aval 2022 Synergistic effects of hybrid (HA+Ag) particles and friction stir processing in the design of a high-strength magnesium matrix bio-nano composite with an appropriate texture for biomedical applications J. Mech. Behav. Biomed. Mater. 125 104983
8. H Aghamohammadi SJ Hosseinipour SM Rabiee R Jamaati 2021 Effect of hot rolling on microstructure, crystallographic texture, and hardness of AZ31 alloy Mater. Chem. Phys. 273 125130
9. F Guo DF Zhang XS Yang LY Jiang FS Pan 2015 Microstructure and texture evolution of AZ31 magnesium alloy during large strain hot rolling Trans. Nonferrous Metals Soc. China 25 14 21
10. MT Perez-Prado JA Valle del JM Contreras OA Ruano 2004 Microstructural evolution during large strain hot rolling of an AM60 Mg alloy Scripta Mater. 50 661 665
11. F Guo D Zhang X Fan J Li L Jiang F Pan 2016 Microstructure, texture and mechanical properties evolution of pre-twinning Mg alloys sheets during large strain hot rolling Mater. Sci. Eng. A 655 92 99
12. H Zhang G Huang L Wang H Jørgen Roven F Pan 2013 Enhanced mechanical properties of AZ31 magnesium alloy sheets processed by three-directional rolling J. Alloy Compd. 575 408 413
13. W Tang S Huang D Li Y Peng 2015 Mechanical anisotropy and deep drawing behaviors of AZ31 magnesium alloy sheets produced by unidirectional and cross rolling J. Mater. Process. Technol. 215 320 326
14. X Li T Al-Samman G Gottstein 2011 Mechanical properties and anisotropy of ME20 magnesium sheet produced by unidirectional and cross rolling Mater. Des. 32 4385 4393
15. T Chen Z Chen L Yi J Xiong C Liu 2014 Effects of texture on anisotropy of mechanical properties in annealed Mg–0.6%Zr–1.0%Cd sheets by unidirectional and cross rolling Mater. Sci. Eng. A 615 324 330
16. E Tolouie R Jamaati 2018 Effect of β–$Mg_{17}Al_{12}$ phase on microstructure, texture and mechanical properties of AZ91 alloy processed by asymmetric hot rolling Mater. Sci. Eng. A 738 81 89
17. S Biswas DI Kim S Suwas 2012 Asymmetric and symmetric rolling of magnesium: evolution of microstructure, texture and mechanical properties Mater. Sci. Eng. A 550 19 30
18. B Beausir S Biswas DI Kim LS Tóth S Suwas 2009 Analysis of microstructure and texture evolution in pure magnesium during symmetric and asymmetric rolling Acta Mater. 57 5061 5077
19. E Tolouie R Jamaati 2023 Effect of rolling reduction on the microstructure, texture, and mechanical behavior of AZ91 alloy J. Market. Res. 26 7947 7957
20. C Xu MY Zheng K Wu ED Wang GH Fan SW Xu S Kamado XD Liu GJ Wang XY Lv MJ Li YT Liu 2013 Effect of final rolling reduction on the microstructure and mechanical properties of Mg–Gd–Y–Zn–Zr alloy sheets Mater. Sci. Eng. A 559 232 240
21. XS Huang K Suzuki A Watazu I Shigematsu N Saito 2009 Effects of thickness reduction per pass on microstructure and texture of Mg–3Al–1Zn alloy sheet processed by differential speed rolling Scripta Mater. 60 964 967
22. MR Ghandehari Ferdowsi M Mazinani GR Ebrahimi 2014 Effects of hot rolling and interstage annealing on the microstructure and texture evolution in a partially homogenized AZ91 magnesium alloy Mater. Sci. Eng. A 606 214 227
23. W Wang W Zhang W Chen G Cui E Wang 2018 Effect of initial texture on the bending behavior, microstructure and texture evolution of ZK60 magnesium alloy during the bending process J. Alloy. Compd. 737 505 514
24. X Yu T Li L Li S Liu Y Li 2017 Influence of initial texture on the shock property and spall behavior of magnesium alloy AZ31B Mater. Sci. Eng. A 700 259 268
25. D Liu Z Liu E Wang 2018 Improving single pass reduction during cold rolling by controlling initial texture of AZ31 magnesium alloy sheet Trans. Nonferrous Metals Soc. China 28 244 250
26. H Zhang G Huang D Kong G Sang B Song 2011 Influence of initial texture on formability of AZ31B magnesium alloy sheets at different temperatures J. Mater. Process. Technol. 211 1575 1580
27. HL Kim WK Bang YW Chang 2012 Effect of initial texture on deformation behavior of AZ31 magnesium alloy sheets under biaxial loading Mater. Sci. Eng., A 552 245 251
28. N Li G Huang R Xin Q Liu 2013 Effect of initial texture on dynamic recrystallization and deformation mechanisms in AZ31 Mg alloy extruded at 573K Mater. Sci. Eng. A 569 18 26
29. B Alili H Azzeddine K Abib D Bradai 2013 Texture evolution in AZ91 alloy after hot rolling and annealing Trans Nonferrous Metals Soc China 23 2215 2221
30. Y Jiang G Tang C Shek W Liu 2011 Microstructure and texture evolution of the cold-rolled AZ91 magnesium alloy strip under electropulsing treatment J. Alloy. Compd. 509 4308 4313
31. F Guo D Zhang H Wu L Jiang F Pan 2017 The role of Al content on deformation behavior and related texture evolution during hot rolling of Mg-Al-Zn alloys J. Alloy. Compd. 695 396 403
32. AM Jorge Jr E Prokofiev MR Martins Triques V Roche WJ Botta CS Kiminami GI Raab TG Langdon 2017 Effect of cold rolling on the structure and hydrogen properties of AZ91 and AM60D magnesium alloys processed by ECAP Int. J. Hydrog. Energy 42 21822 21831

Publisher's Note Springer Nature remains neutral with regard to jurisdictional claims in published maps and institutional affiliations.